

Interaction of a Self-Assembling Peptide with Oligonucleotides: Complexation and Aggregation

Mei Wang,* Maggie Law,* Jean Duhamel,[†] and P. Chen*

Departments of *Chemical Engineering and [†]Chemistry, University of Waterloo, Waterloo, Ontario, Canada

ABSTRACT Molecular interaction of a self-assembling peptide, EAK16-II, to single- and double-stranded oligodeoxynucleotides (ODNs) was investigated under various solution conditions. The molecular events leading to EAK-ODN complexation and further aggregation were elucidated using a series of spectroscopic and microscopic methods. Despite the ability to self-assemble, EAK molecules bind to ODN molecules first upon mixing, resulting in EAK-ODN complexes. The complexes further associate to form EAK-ODN aggregates. A method based on UV-Vis absorption and centrifugation was developed to quantify the fraction of ODNs in the aggregates. The results were used to construct binding isotherms via a binding density function analysis. To compare the effects of different pH values and nucleotide types, the modified noncooperative McGhee and von Hippel model was used to extract binding parameters from the binding isotherms. The binding constant of EAK to ODNs was higher at pH 4 than at pH 7, and no binding was observed at pH 11, indicating that the interaction involved is primarily electrostatic in nature. EAK bound more strongly to single-stranded ODNs. The EAK-ODN aggregates were further visualized using atomic force microscopy; their size distribution as a function of EAK concentration was monitored by dynamic light scattering. The timescale for the EAK-ODN aggregation was on the order of minutes by fluorescence anisotropy and steady-state light scattering experiments. Fluorescence quenching experiments demonstrated that the ODNs in the aggregates were less accessible to the solvent, demonstrating a potential of oligonucleotide encapsulation by the self-assembling peptide.

INTRODUCTION

Self-assembling peptides have recently emerged as one of the most promising biomolecular materials in bio-nanotechnology research (1–5). The self-assembly of peptides not only relates to many naturally occurring states of proteins, such as amyloid fibrillogenesis (4), but also provides useful biomolecular building blocks for a wide variety of supramolecular fabrications (1–3). Among the new self-assembling peptides is a class of ionic-complementary, amphiphilic peptides, e.g., EAK made of glutamic acid (E), alanine (A), and lysine (K) residues (1). This new class of peptides originates from zuotin, a yeast protein that preferentially binds to left-handed Z-DNA (1). The molecular structure of these peptides contains alternating positive and negative charges, enabling ionic-complementarity. This ionic complementarity, together with hydrogen-bonding, hydrophobic, and van der Waals interactions promotes self-assembly of the peptide molecules into highly stable aggregates (2,6,7). The nano/microstructures constructed from the peptide self-assembly have found many biomedical applications, including scaffolding for tissue engineering (8,9) and biological surface patterning (3). It has been shown recently that these peptides can encapsulate a hydrophobic organic compound and unload it into a model cell membrane in a controlled manner (10). It is interesting to see if these self-assembling peptides can also be used for carrying DNA or RNA in gene delivery,

which is the current bottleneck to gene therapy (11,12). Our particular interest is the self-assembling peptide-mediated delivery of antisense oligonucleotides and short-interfering RNAs (siRNAs) (13).

The first key step to develop an oligonucleotide delivery system is to form peptide-oligonucleotide complexes (11,12). This entails the study of the binding of the peptide to oligonucleotides and the conformations of the resulting peptide-oligonucleotide complexes. The peptide and oligonucleotides used in this work are EAK16-II, a well-studied self-assembling peptide (1) referred to as EAK later on, and both single- and double-stranded oligodeoxynucleotides (ODNs), namely a guanine hexadecamer (dG₁₆), a cytosine hexadecamer (dC₁₆), and their duplex (dGC₁₆). It has been argued that many peptide-nucleic acid interactions are not sequence-specific, resulting from noncovalent molecular interactions (14–23). Thus, the dG₁₆ and dC₁₆ hexadecamers were chosen to assess how a purine or a pyrimidine affects the binding of a self-assembling peptide to an oligonucleotide. Since most therapeutic antisense oligonucleotides and siRNAs are short nucleic acids of <22 nucleotides in length, the choice of 16 mers is somewhat arbitrary but within the usual therapeutic oligonucleotide length range.

While there has been no study of binding between self-assembling peptides and oligonucleotides, numerous investigations have been done on the binding between proteins and nucleic acids (11,12,14–32). Characterization of the binding between a ligand protein and a nucleic acid requires the determination of the concentrations of the free and bound species involved. These quantities can be obtained by relating them to changes in the physicochemical or biological

Submitted December 6, 2006, and accepted for publication May 17, 2007.

Address reprint requests to J. Duhamel, E-mail: jduhamel@sciborg.uwaterloo.ca; or P. Chen, E-mail: p4chen@cape.uwaterloo.ca.

Editor: David P. Millar.

© 2007 by the Biophysical Society

0006-3495/07/10/2477/14 \$2.00

doi: 10.1529/biophysj.106.102624

properties resulting from the formation of complexes (23). In most instances, these changes can be probed by techniques such as gel mobility shift assay (24,25), filter binding assay (26), surface plasmon resonance (27), and fluorescence (28,29). These last methods require labeling of the ligand with a chromophore or radioactive isotope, or covalent immobilization of the ligand. Besides being time-consuming, labeling or immobilization of ligands can affect their biochemical activity, resulting in an inaccurate binding isotherm. Other characterization methods, such as boundary sedimentation velocity (30) and UV difference spectra (31), do not require labeling of the molecule of interest, although labeling can be used if the behavior of a specific species needs to be isolated (32).

In this work, UV absorption measurements were adopted in conjunction with centrifugation of solutions of oligonucleotide and peptide, where the concentration of the oligonucleotide left in the supernatant could be determined. This method, also referred to as the depletion method (33), has the advantage of not requiring large quantities of samples or any chemical labeling. As will be shown later, this combination of UV absorption and centrifugation may be used for a wide range of solution systems where both molecular binding and subsequent aggregation occur. Oligodeoxynucleotides naturally exhibit a characteristic absorbance in the UV-Vis range. Upon peptide binding, aggregates made of peptide-ODN complexes formed. These aggregates could be centrifuged out, leaving behind a mixture of unbound ODNs and some EAK-ODN complexes in the supernatant. The concentration of ODN in the supernatant was determined by UV absorption. The experimental results were treated with a binding density function analysis (23,34) to generate isotherms of the binding between peptide and ODNs. The outcome was analyzed further with the modified noncooperative McGhee and von Hippel (MvH) model for the purpose of comparing the effects of solution conditions and ODN types (15,22).

Some unique challenges are encountered when studying the interaction of a self-assembling peptide with an ODN. Since the peptide can self-assemble into nanostructures, EAK nanofibers in the present case (1,7), there is a question as to whether EAK would bind to the ODN molecules directly, or EAK would first self-assemble into its aggregates to which the ODN binds subsequently. This article presents a series of experiments designed to demonstrate that EAK binds to ODNs in molecular form, before the peptide self-assembly takes place. The peptide-ODN aggregates are believed to form after an initial step of molecular binding between peptide and ODN molecules, and a subsequent association of the peptide-ODN (intermediate) complexes into aggregates, possibly assisted by the inherent self-assembly capability of the peptide.

After binding and nanostructure formation with the peptide, the ODN was further evaluated for its accessibility to solvent species by fluorescence quenching experiments, as this property is critically important to assess the stability and

potency of ODNs during their delivery both in vitro and in vivo (11,12). This study represents the first example in the literature where the binding of a self-assembling peptide to oligonucleotides is characterized.

EXPERIMENTAL SECTION

Materials

All reagents were of analytical grade and obtained from BDH (Poole, UK). The pH dependence of the binding of EAK to the ODNs was investigated by performing experiments at three different pH values. The pH 4 buffer was made with 0.171 M acetic acid and 0.029 M sodium acetate adjusted with acetic acid (35); the pH 7 buffer was made with 0.01 M tris(hydroxymethyl)methylamine and 0.005 M sodium sulfate adjusted with sulfuric acid (35); the pH 11 buffer was made with 0.1 M glycine and 0.1 M sodium chloride adjusted with sodium hydroxide (36).

The EAK16-II peptide whose sequence is shown in Table 1 was purchased from CanPeptide (Quebec, Canada) and the C-terminus carboxyfluorescein-labeled EAK (FAM-EAK) were purchased from Research Genetics (Huntsville, AL) and used without further purification.

Four single-stranded oligodeoxynucleotides (ssODNs), namely dG₁₆, dC₁₆, FAM-dC₁₆ (dC₁₆ labeled with carboxyfluorescein at the 5'-end), and dC₁₆-Rh (dC₁₆ labeled with carboxytetramethylrhodamine at the 3'-end) were obtained with 95% purity from Eurogentec North America (San Diego, CA) with HPLC purification. The ODN sequences are listed in Table 1. Solutions of the double-stranded ODNs (dsODNs) at different pHs were prepared one day before use by mixing two equimolar amounts of complementary ssODNs in the corresponding buffer in Eppendorf tubes, placing the tubes in a 95°C water bath for 5 min, turning off the water bath, and letting the solution slowly cool to room temperature.

UV-Vis absorbance

UV-Vis absorption spectra were obtained on a model No. 8452A diode array spectrophotometer (Hewlett-Packard, Palo Alto, CA) using a 50 μL quartz cuvette from Hellma (Müllheim, Germany).

Samples for the construction of binding isotherms were prepared at pH 4, 7, and 11. For each pH, two ODN concentrations of ~3 μM and 7 μM were used. At each ODN concentration, six-to-seven samples were prepared with EAK concentrations ranging from 0 to 0.2 mg/mL (equivalent to 0–120 μM) by mixing the ODN solution with different amounts of EAK powder. The

TABLE 1 Type, name, and sequence of oligonucleotides (ODNs) and self-assembling peptide

Type	Name	Sequence
Single-stranded ODN (ssODN)	dG ₁₆	5'-GGG GGG GGG GGG GGG G-3'
	dC ₁₆	5'-CCC CCC CCC CCC CCC C-3'
	FAM-dC ₁₆	5'-Fluorescein-CCC CCC CCC CCC CCC C-3'
	dC ₁₆ -Rh	5'-CCC CCC CCC CCC CCC C-Rhodamine-3'
Double-stranded ODN (dsODN)	dGC ₁₆	5'-GGG GGG GGG GGG GGG G-3' 3'-CCC CCC CCC CCC CCC C-5'
	FAM-dGC ₁₆	5'-GGG GGG GGG GGG GGG G-3' 3'-CCC CCC CCC CCC CCC C-Fluorescein-5'
	EAK16-II	EAK n-AEAEAKAKAEAEAKAK-c FAM-EAK n-AEAEAKAKAEAEAKAK-c-Fluorescein

resulting solutions were stirred vigorously for a few seconds with a vortex mixer and incubated at 25°C for 30 min. The EAK-ODN aggregates formed in the solution were removed by centrifugation at 14,000 rpm for 2 min with a model No. 5410 centrifuge (Eppendorf, Hamburg, Germany). The supernatant was collected and its absorbance was measured on the spectrophotometer at wavelengths between 190 and 800 nm. Beer's Law was used to determine the total ODN concentration and the concentration of the ODN left in the supernatants from the absorbance of the ODN at 260 nm of the initial solution (OD_o) and the supernatant (OD_s), respectively. The term $(OD_o - OD_s)/OD_o$ was defined as the relative UV-Vis absorbance change ΔOD_r . The obtained ΔOD_r were then analyzed using the ligand binding density function (23) to generate binding isotherms.

Polyacrylamide gel electrophoresis (PAGE)

PAGE was applied to detect whether EAK-dsODN complexes/aggregates were present in the supernatant after centrifugation. Samples containing 3.6 μ M of dGC₁₆ with 0, 0.01, 0.1, or 0.2 mg/mL (0, 6, 60, or 120 μ M) of EAK were prepared at pH 4 and 7. The supernatants obtained by centrifuging the samples were analyzed with nondenaturing 20% PAGE. The polyacrylamide gels were 14-cm long \times 15-cm wide \times 0.5-mm thick. PAGE was performed in the corresponding buffer at 10 V/cm for 2 h. The gels were stained with a solution of 0.5 mg/mL ethidium bromide for 30 min before being visualized with a UV Transilluminator gel document system (Bio-Rad, Hercules, CA).

Steady-state fluorescence

Fluorescence spectra of dC₁₆ labeled with carboxyfluorescein at the 5'-end (FAM-dC₁₆), dC₁₆ labeled with carboxytetramethylrhodamine at the 3'-end (dC₁₆-Rh), and EAK labeled with carboxyfluorescein at the C-terminus (FAM-EAK) were acquired on a steady-state fluorometer (Photon Technology International, Birmingham, NJ) equipped with a Ushio UXL-75Xe Xenon arc lamp and PTI 814 photomultiplier detection system. The peak absorption wavelength of the solution was chosen as the excitation wavelength (μ_{ex}). For the FAM-dC₁₆ and FAM-EAK solutions, μ_{ex} was 452 nm at pH 4 and 494 nm at pH 7, respectively; for the dC₁₆-Rh solutions, μ_{ex} was 560 nm at both pH 4 and pH 7.

Steady-state fluorescence anisotropy

Anisotropy of the supernatants obtained after centrifuging the solutions was measured using the steady-state fluorometer with polarizers fitted on the excitation and emission monochromators. Each sample was excited with vertically polarized light, and the fluorescence intensity was separately detected with the emission polarizer set in the vertical (I_{VV}) and horizontal (I_{VH}) orientations. In a fluorescence anisotropy experiment, the polarization dependence of the emission monochromator was corrected by the G factor (37). To obtain the G factor, the excitation polarizer was set to the horizontal direction, and the fluorescence intensities were measured individually with vertical (I_{HV}) and horizontal (I_{HH}) emission polarization. The G factor is given by the I_{HV}/I_{HH} ratio. The fluorescence anisotropy (r) was calculated using Eq. 1 (37):

$$r = \frac{I_{VV} - GI_{VH}}{I_{VV} + 2GI_{VH}} \quad (1)$$

The wavelength corresponding to the maximum absorption of FAM was chosen as the excitation wavelength (μ_{ex}). The fluorescence intensity was monitored at 514 nm, the peak wavelength of the emission spectra.

Time-resolved fluorescence decays

Fluorescence decays were acquired by the time-correlated single photon counting technique on a time-resolved fluorometer (IBH System 2000,

Glasgow, UK). Samples containing 3.6 μ M of the chromophore-labeled dC₁₆ were prepared in the presence and the absence of 0.2 mg/mL (120 μ M) EAK at pH 4. The excitation wavelength (μ_{ex}) and emission wavelength (μ_{em}) were set to the wavelength corresponding to the absorption and emission maxima of the chromophores. For FAM-dC₁₆, μ_{ex} and μ_{em} were 452 nm and 514 nm, respectively; for dC₁₆-Rh, μ_{ex} and μ_{em} were 560 nm and 580 nm, respectively. A right-angle configuration was used between the excitation and emission monochromators. All decay curves were collected over 512 channels and with a total of 20,000 counts in the channel of maximum intensity. The analysis of the decay curves started by acquiring the instrument response function obtained with a scattering solution, which was then convoluted with a sum of exponentials shown in Eq. 2 (37)

$$I(t) = \sum_{i=1}^N \alpha_i e^{-t/\tau_i}, \quad (2)$$

where $i = 1, 2, \dots, N$; N is the minimum number of exponentials required to achieve a good fit. The fitting parameters were optimized using the Marquardt-Levenberg algorithm (38). The fits of the fluorescence decays were deemed satisfactory when the μ^2 value was smaller than 1.3 and the residuals and autocorrelation function of the residuals were randomly distributed around zero.

Steady-state light scattering (SLS)

SLS intensity of solutions of EAK, ODNs, and their mixtures was monitored at right angle with the steady-state fluorometer by irradiating the solution at 350 nm where the ODNs and EAK do not absorb or emit.

Dynamic light scattering (DLS)

The hydrodynamic diameter of the EAK-ODN complexes/aggregates in the pH 4 buffer was obtained with a Zetasizer Nano ZS instrument equipped with a 4 mW He-Ne laser operating at 633 nm (Malvern Instruments, Malvern, Worcestershire, UK). All measurements were performed at 25°C at a measurement angle of 173°. Dust particles were found to be absent in the buffer solutions used to prepare the samples, as confirmed by dynamic light scattering. DLS experiments were performed 30 min after sample preparation.

Atomic force microscopy (AFM)

A Picoscan atomic force microscope (Molecular Imaging, Tempe, AZ) was used to study the morphology of the EAK-ODN complexes/aggregates in solution. It was operated in magnetic AC tapping mode in solution using magnetically coated cantilevers, Type II MAClevers (Molecular Imaging), with a spring constant of 0.5 N/m and a resonance frequency of \sim 27 kHz at room temperature. A volume of 400 μ L of each solution was deposited on a freshly cleaved mica surface, inside a Teflon liquid chamber, where the AFM images were acquired.

THEORETICAL BACKGROUND

As will be shown in Results and Discussion, interaction of EAK with ODN results in aggregates composed of EAK and ODN. The fraction of ODNs in the aggregates can be obtained from the relative change in absorbance, ΔOD_r , described in the Experimental Section. It has been shown (39,40) that the fraction of ODN in aggregates is a unique function of binding density (ν , which is in turn a sole function of free ligand concentration (P_f)). The binding density, ν , is defined as (15,41)

$$\nu = P_b/D_t, \quad (3)$$

with P_b being the concentration of the total bound peptide and D_t the total ODN concentration expressed in terms of phosphate groups. Thus, ΔOD_r is a unique function of P_f . The ligand binding density function proposed by Bujalowski and Lohman (23,34) can be adopted to construct a binding isotherm by creating a data set (ν, P_f). This procedure is described in more detail in Section S.A of the Supplementary Material. Briefly, for any given ΔOD_r , Eq. 4 relates P_f to the total peptide concentration and the total ODN concentration

$$P_{tx} = P_f + \nu D_{tx}, \quad (4)$$

where P_{tx} and D_{tx} represent the concentrations of total peptide and total ODN at the x^{th} ODN concentration (there are four ODN concentrations for each system, see Fig. 1), respectively. Since P_f and ν are constant values for a given ΔOD_r , the binding density ν can be obtained from the slope of the plot of P_t versus D_t .

The procedure for building binding isotherms consists of using three or four ODN concentrations and plotting the fraction of ODN in the aggregates, i.e., ΔOD_r , as a function of the total peptide concentration (Fig. 1). Each plot could be fitted reasonably well with the equation $\Delta OD_r = A \times P_t / (I + B \times P_t)$, where A and B are regression parameters listed in Table 2. In this article, sets of ν and P_f were obtained from the plot of P_t versus D_t for a given ΔOD_r . Seven-to-ten ΔOD_r values were chosen. For each ΔOD_r value, the value of P_t was read from the fits of the curves shown in Fig. 1 and plotted as a function of D_t . Then P_f and ν were obtained from the intercept and slope of the plot of P_t versus D_t . Plotting ν/P_f versus ν generated the binding isotherms (Fig. 2). The interaction/binding between EAK and ODN molecules most likely starts with the formation of EAK-ODN complexes as will be argued in Results and Discussion, which is followed by further association of the complexes into aggregates. This process is described in Scheme I,



where K_c and K_a are the equilibrium constants for the formation of EAK-ODN complexes from unimolecular ODN and EAK and for the formation of EAK-ODN aggregates from the association of EAK-ODN complexes, respectively. One important aspect of the procedure described above is that, although ΔOD_r represents the fraction of ODNs present in the aggregates and does not account for the ODNs present in the supernatant as EAK-ODN complexes, ΔOD_r is still a unique function of P_f and ν as demonstrated by the work of Teif et al. (39,40).

No suitable theoretical model could be found in the literature to describe the molecular binding (K_c) and aggregation (K_a) simultaneously. To do so, an isotherm would have to be

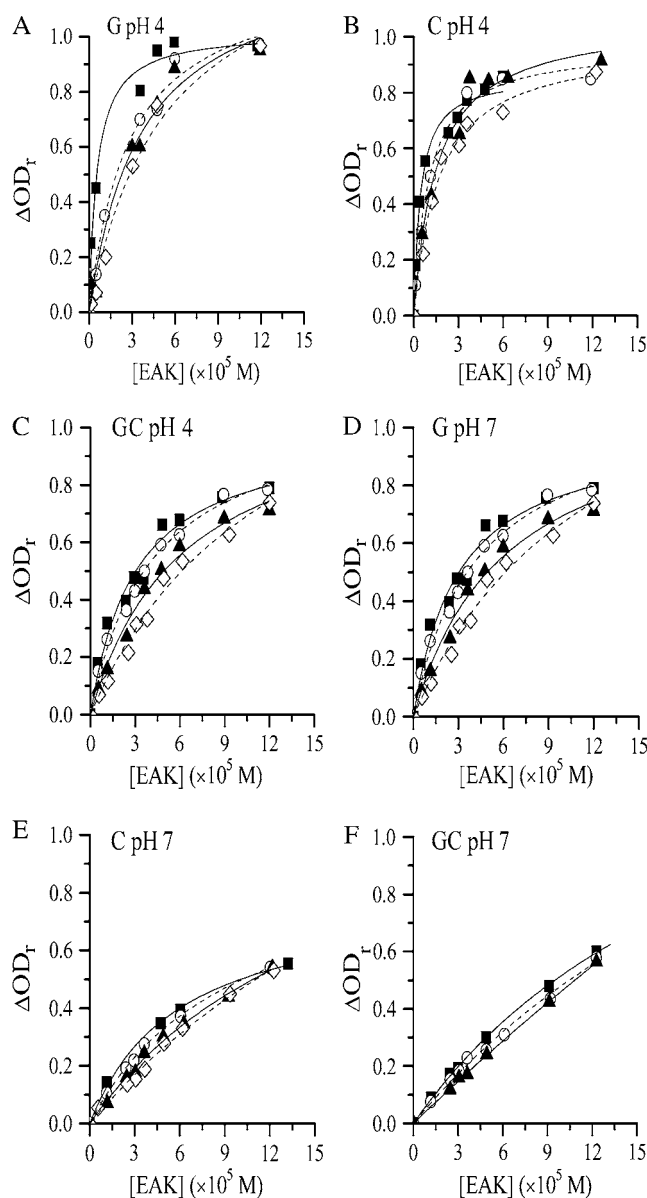


FIGURE 1 Plots of ΔOD_r as a function of the total EAK concentration. (A) pH 4, phosphate concentration of dG₁₆ equals 32 μM (■), 64 μM (○), 94.4 μM (▲), and 152 μM (◇). (B) pH 4, phosphate concentration of dC₁₆ equals 24 μM (■), 48 μM (○), 90 μM (▲), and 116.8 μM (◇). (C) pH 4, phosphate concentration of dGC₁₆ equals 64 μM (■), 128 μM (○), 240 μM (▲), and 288 μM (◇). (D) pH 7, phosphate concentration of dG₁₆ equals 16 μM (■), 32 μM (○), 64 μM (▲), and 96 μM (◇). (E) pH 7, phosphate concentration of dC₁₆ equals 16 μM (■), 32 μM (○), 64 μM (▲), and 96 μM (◇). (F) pH 7, phosphate concentration of dGC₁₆ equals 32 μM (■), 64 μM (○), and 128 μM (▲). The solid and dashed lines represent the best fits to the equation $\Delta OD_r = A \times [EAK] / (I + B \times [EAK])$, but do not have any physical meaning. The A and B parameters have been listed in Table 2. Data in the range of 20–70% of maximal ΔOD_r are used to obtain the ν and ν/P_f values reported in Fig. 2.

constructed for each of the two steps. To facilitate the analysis of the binding isotherms, i.e., the ν/P_f versus ν trends shown in Fig. 2, the modified noncooperative McGhee and von Hippel (MvH) model (15,22) was used:

TABLE 2 Parameters A and B retrieved from the fits of the ΔOD_r versus [EAK] plots shown in Fig. 1 with the empirical equation: $\Delta OD_r = A \times [EAK]/(1+B \times [EAK])$

pH 4		dG ₁₆			
Concentration	2.0 μ M	4.0 μ M	5.9 μ M	9.5 μ M	
A (10^4)	18.454 \pm 3.465	4.513 \pm 0.507	3.574 \pm 0.613	2.846 \pm 0.248	
B (10^4)	18.088 \pm 3.853	3.645 \pm 0.599	2.750 \pm 0.751	2.053 \pm 0.306	
pH 4		dC ₁₆			
Concentration	1.5 μ M	3.0 μ M	5.0 μ M	7.3 μ M	
A (10^4)	19.262 \pm 2.549	9.747 \pm 0.981	6.954 \pm 1.074	5.871 \pm 0.583	
B (10^4)	22.309 \pm 3.481	10.073 \pm 1.249	6.547 \pm 1.328	5.996 \pm 0.823	
pH 4		dG ₁₆			
Concentration	2.0 μ M	4.0 μ M	7.5 μ M	9.0 μ M	
A (10^4)	4.871 \pm 0.671	2.436 \pm 0.414	1.599 \pm 0.153	1.247 \pm 0.140	
B (10^4)	5.539 \pm 1.048	2.440 \pm 0.670	1.367 \pm 0.254	0.878 \pm 0.236	
pH 7		dG ₁₆			
Concentration	1.0 μ M	2.0 μ M	4.0 μ M	6.0 μ M	
A (10^4)	3.309 \pm 0.387	2.612 \pm 0.176	1.834 \pm 0.163	1.237 \pm 0.095	
B (10^4)	3.318 \pm 0.587	2.425 \pm 0.269	1.636 \pm 0.267	0.844 \pm 0.160	
pH 7		dC ₁₆			
Concentration	1.0 μ M	2.0 μ M	4.0 μ M	6.0 μ M	
A (10^4)	1.341 \pm 0.082	1.001 \pm 0.027	0.752 \pm 0.036	0.621 \pm 0.034	
B (10^4)	1.686 \pm 0.175	1.035 \pm 0.063	0.585 \pm 0.085	0.339 \pm 0.081	
pH 7		dGC ₁₆			
Concentration	1.0 μ M	2.0 μ M	4.0 μ M		
A (10^4)	0.748 \pm 0.019	0.631 \pm 0.035	0.503 \pm 0.011		
B (10^4)	0.442 \pm 0.038	0.306 \pm 0.077	0.082 \pm 0.023		

$$\frac{\nu}{P_f} = K(1 - n\nu) \left(\frac{1 - n\nu}{1 - (n-1)\nu} \right)^{(n-1)} \left(\frac{N - n + 1}{N} \right). \quad (5)$$

It was noted that the MvH model describes the initial complexation process only, and does not take into account the second aggregation step. Nevertheless, we opted to use the MvH model for the following reasons: First, the main goal of the current study was to find differences or similarities in the process leading to the formation of EAK-ODN aggregates under different experimental conditions, e.g., pH values and nucleotide types; in other words, the MvH model is used for comparison purpose, as has been practiced before (42).

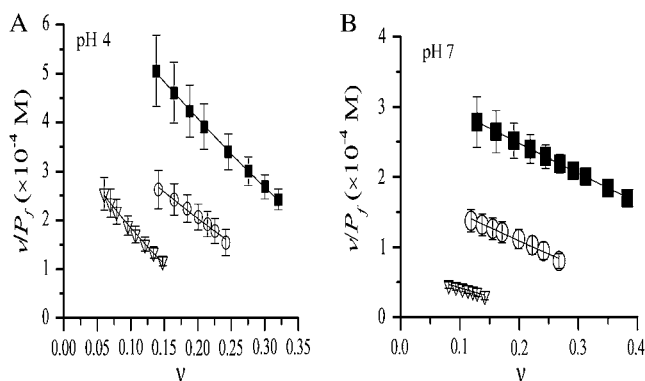


FIGURE 2 Plot of ν/P_f versus ν for the binding of EAK to dG₁₆ (■), dC₁₆ (○), and dGC₁₆ (▽) at (A) pH 4 and (B) pH 7. The solid lines represent the best fits to Eq. 5. The parameters used in the fits are listed in Table 3.

Second, the binding constant K calculated from the MvH model actually shows trends for the binding strength of EAK to different ODNs and under various solution conditions, which are also comparable with those reported for the binding of other DNA/peptide pairs. With these considerations, the binding isotherms shown in Fig. 2 were fitted with Eq. 5.

RESULTS AND DISCUSSION

This study aims at describing the interaction of EAK with ODNs. To reach this goal, several issues were addressed by carrying out a number of separate experiments. Each issue is treated in a separate chapter of this section. The structure of this section is briefly laid out here. First, proof of the binding of EAK to the ODNs was obtained by conducting absorption measurements on the supernatant of centrifuged solutions of the EAK-ODN mixtures. Second, PAGE, fluorescence anisotropy, and UV-Vis absorption measurements were conducted to confirm that the quantity ΔOD_r is an appropriate representation of the fraction of ODNs incorporated in the EAK-ODN aggregates. Third, fluorescence anisotropy and steady-state light scattering experiments established that the timescale over which the EAK-ODN aggregates form is much shorter than that over which the self-assembly of EAK occurs. Fourth, the size of the EAK-ODN aggregates was determined using AFM and dynamic light scattering. Fifth, the modified MvH model was used to compare the binding of EAK to the ODNs under different pHs and nucleotide types. Sixth, the accessibility of the ODNs to the solvent once

encapsulated inside the EAK-ODN aggregates was investigated by performing fluorescence quenching experiments.

Effect of pH on binding

EAK contains four glutamic acids (Glu, E) and four lysines (Lys, K) with pK_a values of 4.25 and 10.53, respectively (43). The carboxylic acid of Glu and the amine of Lys are negatively and positively charged at pH 7, respectively. Therefore, EAK exhibits alternating negative and positive charges along its backbone at pH 7. Since glutamic acid residues are mostly protonated under acidic conditions at pHs below 4.25, EAK molecules are expected to be positively charged at pH 4. Similarly Lys becomes neutral at pHs above 10.53, so that EAK molecules are expected to be negatively charged at pH 11. Since the binding of negatively charged ODNs to cationic molecules, such as lysine-rich peptides, is believed to be due to electrostatic attraction (44), the different charges born by EAK at different pHs should affect the binding of EAK to the ODNs, with a higher binding constant being expected at lower pHs. To check whether this prediction is correct, the binding of EAK to dC₁₆, dG₁₆, and dGC₁₆ was monitored at pH 4, 7, and 11. Solutions were prepared with different EAK concentrations at two ODN concentrations. The absorbance of the solution supernatant was measured after the EAK-ODN aggregates had been centrifuged out. The relative change in absorbance, ΔOD_r , was calculated by following the procedure described in the Experimental Section. Plots of ΔOD_r as a function of the total EAK concentration were generated for each ODN concentration at pH 4 and 7 (Fig. 1).

In Fig. 1, ΔOD_r is found to increase with increasing total EAK concentration, eventually leveling off for the single-stranded dG₁₆ and dC₁₆ at pH 4. This trend indicates that more EAK binds to the ODNs upon increasing the EAK concentration, until the ssODNs are saturated. ΔOD_r increases with increasing EAK concentration at pH 7 for both the ssODNs and the dsODN; however, it requires higher EAK concentration to reach the plateau. Furthermore at a given ODN concentration, the ΔOD_r values at pH 7 are significantly lower than those at pH 4. These results suggest that increasing the pH from 4 to 7 results in a much weaker binding between EAK and the ODNs. At pH 11, no binding of EAK to the ODNs could be detected as the EAK concentration was varied from 0 to 120 μ M and ΔOD_r equaled zero. Considering that the charge of EAK is changed from positive to neutral, and then to negative when the pH is increased from 4 to 7, and then to 11, the trends shown in Fig. 1 confirm the important role played by the electrostatic forces in the binding of EAK to the ODNs.

Fig. 1 also shows the effect of the nucleotide type on binding. The ΔOD_r values for dG₁₆ are higher than those for dC₁₆ at a given EAK concentration, implying that more EAK binds to dG₁₆ than to dC₁₆. The ΔOD_r values for the ssODNs are always higher than those obtained for the dGC₁₆ duplex

at the same EAK concentration, suggesting that EAK molecules bind more strongly to the ssODNs than to the dsODN.

Nature of the ODNs remaining in the supernatant after centrifugation

The fraction of the ODN in the EAK-ODN aggregates was determined from the relative UV absorbance change of the solution, ΔOD_r , by assuming that no EAK-ODN aggregates remained in the supernatant after centrifugation. The validity of this assumption was verified first by fluorescence anisotropy experiments.

Fluorescence anisotropy reflects changes in the rotational correlation time of a chromophore, which is related to the hydrodynamic volume of the species to which the chromophore is attached. Larger particles have a longer rotational correlation time, hence a larger anisotropy (37). Solutions containing 3.6 μ M of FAM-dGC₁₆ or of FAM-dC₁₆ were mixed at pH 4 and pH 7 with EAK concentrations ranging from 0 to 0.2 mg/mL (0–120 μ M). The solutions were centrifuged and the fluorescence anisotropy of the supernatants was measured. The anisotropy of the supernatants was plotted in Fig. 3 as a function of EAK concentration. The

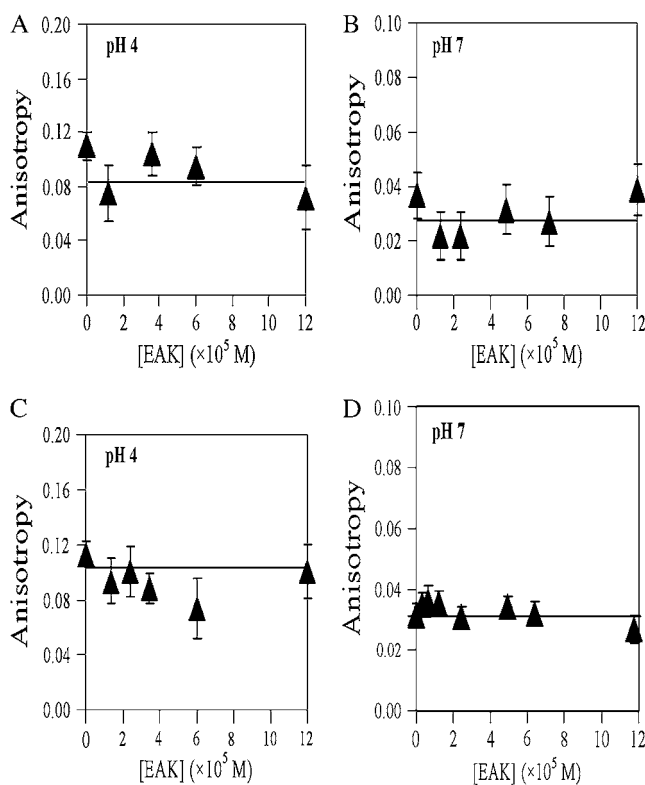


FIGURE 3 Fluorescence anisotropy of the supernatant of EAK solution mixed with 3.6 μ M of (A) FAM-dGC₁₆ at pH 4 (λ_{ex} = 452 nm, λ_{em} = 514 nm), (B) FAM-dGC₁₆ at pH 7 (λ_{ex} = 494 nm, λ_{em} = 514 nm), (C) FAM-dC₁₆ at pH 4 (λ_{ex} = 452 nm, λ_{em} = 514 nm), and (D) FAM-dC₁₆ at pH 7 (λ_{ex} = 494 nm, λ_{em} = 514 nm).

fluorescence anisotropy of FAM-labeled ODNs equals 0.11 ± 0.01 and 0.04 ± 0.01 at pH 4 and pH 7, respectively. It does not equal zero as expected for a free chromophore, because FAM cannot rotate freely and rapidly when it is covalently bound to ODNs. The difference in anisotropy for FAM-ODN at pH 4 and 7 might be due to the shift of the peak absorption wavelength of FAM-ODN from 452 to 494 nm when the pH of the solution is raised from 4 to 7. When the FAM-labeled ODN solution was mixed with increasing EAK concentrations, the anisotropy of the FAM-labeled ODN species left in the supernatants ranged from 0.08 to 0.12 and 0.03 to 0.04 at pH 4 and pH 7, respectively, which was very close to that of the FAM-labeled ODN. These experiments indicate that, within the limit of accuracy of fluorescence anisotropy, the hydrodynamic volume of the fluorescently-labeled species present in the supernatant of the EAK-ODN solutions remains the same as that of FAM-ODN. The results demonstrate that unimers of ODN existed in the centrifuged solutions; no EAK-ODN aggregates were detected.

To estimate the resolution limit of the fluorescence anisotropy experiments, the anisotropy of a $1 \mu\text{M}$ solution of FAM-dC₁₆ was measured as a function of EAK concentration at pH 4 and was plotted in Fig. S.B1 in the Supplementary Material. With the *K*- and *n*-values (Table 3) retrieved from the analysis of the binding isotherms (Fig. 2) using Eq. 5, the fraction of ODNs incorporated in the EAK-ODN aggregates could be calculated and is also plotted in Fig. S.A1. It was found that ~ 10 mol % of ODNs needs to be present in the EAK-ODN aggregates to induce a detectable change in fluorescence anisotropy. Consequently the small anisotropy found in Fig. 3 suggests that if EAK-ODN aggregates are left in the supernatant, they account for <10 mol % of the total ODN population. In other words, ΔOD_r shown in Fig. 1 is an accurate representation of the fraction of ODNs in the EAK-ODN aggregates within ± 10 mol %.

UV-Vis absorption experiments were performed to demonstrate the existence of EAK-ODN complexes in the supernatant that were not detected in the anisotropy experiments. The absorption spectra of the samples containing $3.9 \mu\text{M}$ of dC₁₆-Rh in the presence and absence of $60 \mu\text{M}$ EAK were acquired before and after centrifugation. As shown in Fig. 4, the absorption spectrum of a mixture of dC₁₆-Rh and EAK is different from that of free dC₁₆-Rh. Mixing dC₁₆-Rh with EAK induced a decrease in the absorbance at the 563-nm band characteristic of dC₁₆-Rh, and a new prominent absorption band at 524 nm. The ratio of absorbance at 524

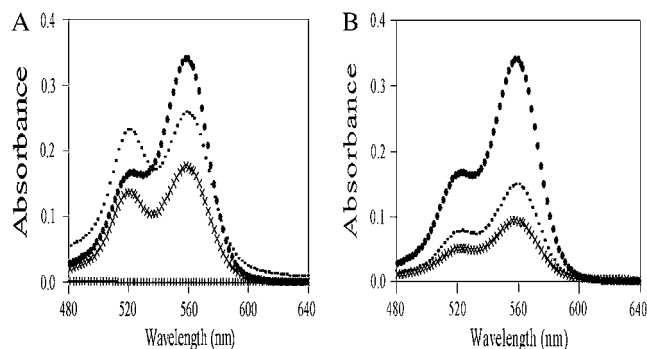


FIGURE 4 UV absorption spectra of dC₁₆-Rh in the presence and absence of EAK at pH 7. (A) $3.9 \mu\text{M}$ dC₁₆-Rh (●), $60 \mu\text{M}$ EAK (+), $3.9 \mu\text{M}$ dC₁₆-Rh and $60 \mu\text{M}$ EAK before centrifugation (—) and after centrifugation (×); (B) dC₁₆-Rh at concentration of $3.9 \mu\text{M}$ (●), $2.0 \mu\text{M}$ (—), and $1.3 \mu\text{M}$ (×).

and 563 nm (OD_{524}/OD_{563}) for dC₁₆-Rh is 0.50 ± 0.01 and is concentration-independent as shown in Fig. 4 B. This ratio changes to 0.89 and 0.78 after mixing with EAK, before and after centrifugation, respectively. Since EAK does not absorb where dC₁₆-Rh does, the spectra and ratio of OD_{524}/OD_{563} for the mixtures would not be different from that of dC₁₆-Rh alone if there were no complexation between EAK and dC₁₆-Rh. The increase in the ratio of OD_{524}/OD_{563} might be due to the dimer formation of rhodamine (45,46) after EAK complexed with dC₁₆-Rh. Since most aggregates are centrifuged out and the ratio of OD_{524}/OD_{563} after centrifugation is similar to that before centrifugation, what remains in the supernatant causing the higher OD_{524}/OD_{563} ratio must be complexes, which are too small to be centrifuged out.

Using the extinction coefficients of the rhodamine dimer reported in the literature (45), the data given in Fig. 4 A can be analyzed to estimate the concentrations of ODNs present in the solution as unimers ($1.39 \mu\text{M}$), complexes ($1.63 \mu\text{M}$), and aggregates ($0.88 \mu\text{M}$). In this situation, ΔOD_r would equal $(0.88 \mu\text{M})/(3.9 \mu\text{M}) = 0.23$, close to the value of 0.28 obtained from the *K* and *n* values listed in Table 3. The agreement observed between the ΔOD_r values obtained through two different means supports the protocol discussed in the Theoretical Background for analyzing the UV-Vis binding results (Fig. 2).

Despite the substantial amount of complexes remaining in the supernatant after centrifugation, no increase in anisotropy was observed in the supernatant (Fig. 3 C), whereas the

TABLE 3 Binding constant *K* and binding site size *n* retrieved from the fits of the data shown in Fig. 2 with Eq. 5

ODNs	pH 4		pH 7		pH 11
	<i>n</i>	<i>K</i> (10^4 M^{-1})	<i>n</i>	<i>K</i> (10^4 M^{-1})	<i>N K</i> (M^{-1})
dG ₁₆	1.66 ± 0.05	7.6 ± 1.2	1.16 ± 0.1	3.4 ± 0.5	No interaction
dC ₁₆	1.96 ± 0.02	4.7 ± 0.6	1.63 ± 0.03	2.0 ± 0.2	No interaction
dGC ₁₆	3.16 ± 0.2	4.2 ± 0.8	2.6 ± 0.3	0.7 ± 0.02	No interaction

Each fit has $R^2 > 0.94$ with at least five data points.

presence of aggregates in the solution results in an observable increase in the anisotropy of the solution (Fig. S.A1). These observations suggest that the aggregates are much larger and more compact than the complexes, resulting in reduced mobility of the fluorescein label. More importantly, they highlight the structural difference between the flexible complexes and the large, compact and rigid aggregates.

Nondenaturing PAGE experiments were further conducted to investigate the nature of dsODN in the supernatant after centrifugation. Samples containing $3.6 \mu\text{M}$ of dGC_{16} mixed with 0, 6, 60, or $120 \mu\text{M}$ of EAK were centrifuged and their supernatants were run on a 20% native gel at pH 4 and pH 7. As shown in Fig. 5 A, for the gel obtained at pH 4 and stained with ethidium bromide, the bands corresponding to the supernatants of EAK- dGC_{16} mixtures (Lanes 2–4) appear at the same position as the band corresponding to dGC_{16} (Lane 1). A similar observation was obtained for the gel run at pH 7 with the EAK- dGC_{16} mixtures (Fig. 5 B). These results suggest that no EAK- dGC_{16} aggregates of a size equivalent to 6–100 basepair duplexes (47) (i.e., the basepair range of a 20% polyacrylamide gel) remain in the supernatants after centrifugation.

The above three experiments have shown that the centrifugation has separated the EAK-ODN aggregates from the original EAK-ODN solution. In the supernatant, there exist free EAK and ODN molecules, as well as EAK-ODN complexes. The fact that the complexes were not detected in either PAGE or anisotropy experiments is due to the inherent resolution limits of the anisotropy and PAGE experiments.

Pathway of the EAK-ODN binding

Considering that EAK in solution has the potential to self-assemble and form aggregates, two most likely pathways can be proposed for the formation of EAK-ODN aggregates. In Pathway 1, EAK self-assembles into aggregates onto which the ODNs bind to form the EAK-ODN aggregates. In Pathway 2, the self-assembly of EAK occurs on a timescale much

longer than the binding of molecular EAK onto ODNs. In this case, the complexation of molecular EAK with ODN molecules occurs first, and is followed by the association of these complexes into aggregates. To identify which pathway is leading to the formation of EAK-ODN aggregates, the timescale over which EAK self-assembles in solution was estimated. To this end, the fluorescence anisotropy of EAK and EAK- dG_{16} mixtures was measured at pH 4 and 7 over a 1 h period immediately after sample preparation using carboxyfluorescein-labeled EAK (FAM-EAK). These experiments were performed with 0.1 mg/mL ($60 \mu\text{M}$) EAK solutions where 1 in 100 EAK molecules was fluorescently labeled. To these solutions, $5 \mu\text{M}$ of dG_{16} was added. The steady-state fluorescence anisotropy of EAK and the EAK- dG_{16} mixtures was measured at pH 4 and 7 as a function of time. The results are shown in Fig. 6, A and B. Whether at pH 4 or 7, the fluorescence anisotropy of FAM-EAK alone remains constant as a function of time and equals 0.10 and 0.05, respectively. This trend indicates that EAK does not self-assemble in solution within a 1 h period, at least to the resolution limit of the anisotropy measurements. This observation is consistent with the results on the hydrodynamic diameter of EAK measured by DLS (see below). On the other hand, addition of dG_{16} to the EAK solution results in a large increase in anisotropy, which reflects a large increase in the hydrodynamic volume of the species present in solution. These species are the EAK-ODN aggregates which may be centrifuged out.

The interaction between individual EAK and ODN molecules was further confirmed by SLS experiments on EAK and EAK- dG_{16} mixtures. The light scattered by the EAK solution remained constant within the first 20 min at pH 4 and pH 7 as shown in Fig. 7, A and B, respectively. As a control, the light scattered by dG_{16} in the buffer solution and by the buffer solution alone was also monitored for 20 min. The SLS intensity of both solutions remained constant and close to the SLS intensity of the solution containing EAK only. These results indicate that the size of EAK remains

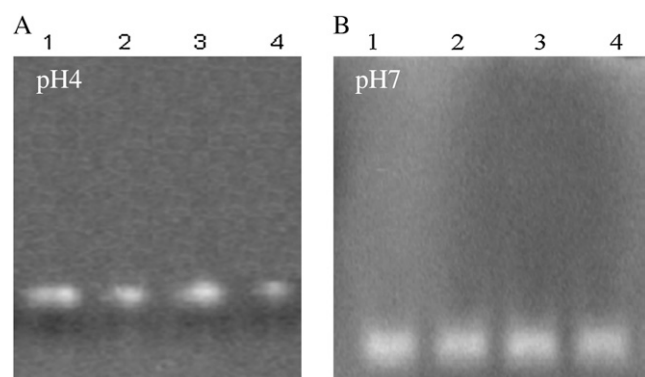


FIGURE 5 20% PAGE of $3.6 \mu\text{M}$ of dGC_{16} mixed with EAK at (A) pH 4 and (B) pH 7. The EAK concentrations are 0, 6, 60, $120 \mu\text{M}$ in lanes 1, 2, 3, and 4, respectively.

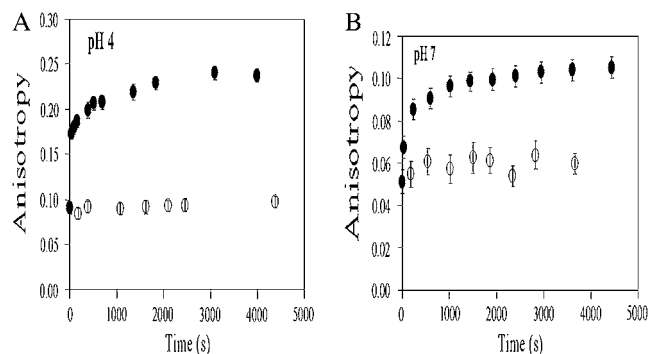


FIGURE 6 Fluorescence anisotropy of a 0.1 mg/mL EAK solution containing 1 mol % of FAM-EAK in the presence (●) and in the absence (○) of (A) $3.6 \mu\text{M}$ of dG_{16} at pH 4 ($\lambda_{\text{ex}} = 452 \text{ nm}$ and $\lambda_{\text{em}} = 514 \text{ nm}$) and (B) $4.3 \mu\text{M}$ of dG_{16} at pH 7 ($\lambda_{\text{ex}} = 494 \text{ nm}$ and $\lambda_{\text{em}} = 514 \text{ nm}$).

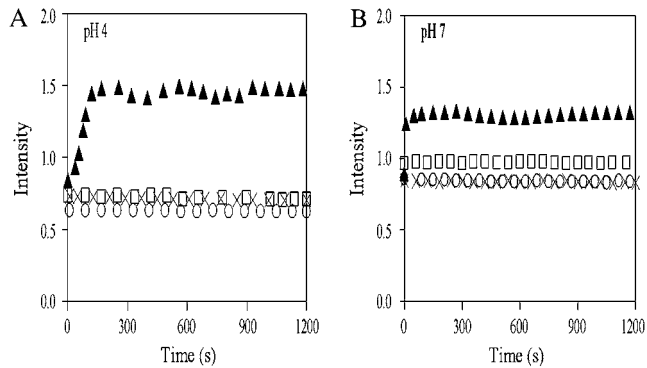


FIGURE 7 SLS experiments performed on (○) the buffer and on solutions containing (▲) 3.6 μM dG₁₆ and 0.1 mg/mL EAK; (□) 0.1 mg/mL EAK; and (×) 3.6 μM dG₁₆ at (A) pH 4 and (B) pH 7. $\lambda_{\text{ex}} = \lambda_{\text{em}} = 350$ nm.

constant during the first 20 min after sample preparation. In comparison, the SLS intensity of the EAK-ODN mixtures increased initially and then leveled off within 30 min at both pHs. Since an increase in SLS intensity reflects an increase in particle size, these results confirm that the size of the complexes/aggregates increases up to a plateau ~ 30 min after mixing, a conclusion similar to that drawn from the anisotropy experiments (Fig. 6). It is noted that the timescales for the formation of EAK-ODN aggregates shown in Figs. 6 and 7 are slightly different. This is due to experimental delays between the time the EAK-ODN mixture was prepared and the measurement was conducted, which resulted in inaccuracy for the first 5 min. However, one can still conclude that the timescale for the formation of EAK-ODN aggregates is much shorter than EAK self-assembly.

Size characterization of EAK-ODN aggregates by AFM and DLS

The size of the EAK-ODN aggregates was characterized using AFM and DLS. Images of the dG₁₆-EAK solution taken 8 and 60 min after sample preparation are shown in Fig. 8. Both small fibers and large aggregates were found after 8 and 60 min and the sizes of these objects did not change during the 1 h time period. The zoomed in view of the image taken at 60 min shows that the smaller fibers are 10-nm wide, 5.2-nm tall, and over 100-nm long. The large aggregates appear to be giant clusters of small fibers with lateral dimensions of 650 nm and a height of 35 nm. Two control experiments were performed: No nanostructure could be detected when a 2 μM dG₁₆ solution was imaged by AFM. Sparsely distributed globular structures with a diameter of 34 nm and a height of 1 nm were observed for the 0.1 mg/mL (60 μM) EAK solution 45 min after solution preparation, which indicated that the majority of EAK molecules do not self-assemble into fibers (images shown in Section S.C of the Supplementary Material). The small fibers and giant aggregates observed in the AFM images of the

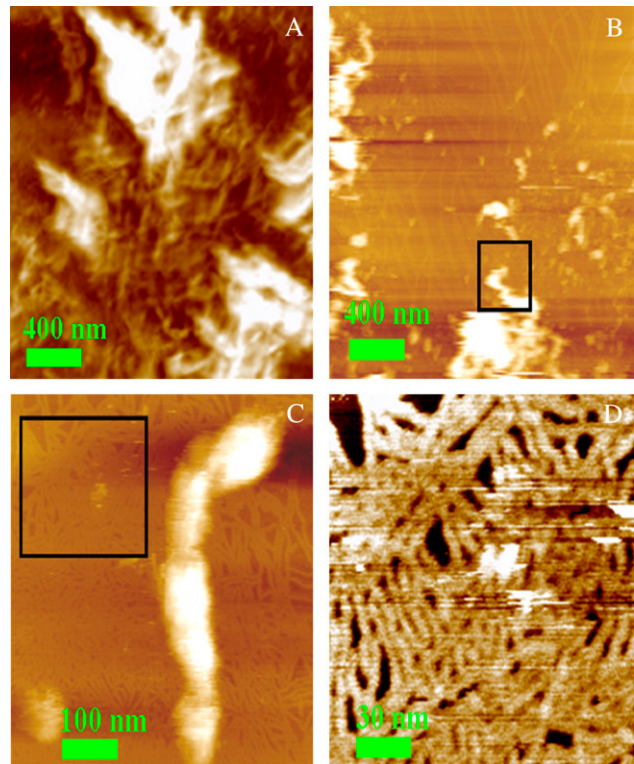


FIGURE 8 AFM images of the EAK-ODN complexes formed in a solution containing 3.6 μM dG₁₆ and 0.1 mg/mL EAK. The complexes were imaged in solution at pH 4. (A) 8 min, (B) 60 min, (C) 70 min, and (D) 75 min. Images in panels C and D are zoomed-in views of the marked areas in panels B and C, respectively.

EAK-dG₁₆ solution are likely due to the association of the EAK-ODN complexes into aggregates. Since the morphologies of the large aggregates observed after 8 and 60 min are very similar, it suggests that the entire complexation process between dG₁₆ and EAK is complete within a short time period, <10 min, which agrees with the conclusions drawn from the anisotropy (Fig. 6) and SLS (Fig. 7) results.

In addition, the hydrodynamic diameter of the EAK-ODN aggregates in solution was obtained by DLS. The hydrodynamic diameter of the EAK-dG₁₆ aggregates at pH 4 with varying concentrations of EAK was measured 30 min after sample preparation (Fig. 9). The dG₁₆ solutions at 7.2 μM exhibited a species with a hydrodynamic diameter of ~ 7.5 nm which was attributed to isolated ODNs in solution. The diameter of the species present in the dG₁₆ solution increased to ~ 150 nm upon adding EAK and remained constant as the EAK concentration was increased from 0.01 to 0.04 mg/mL (6–24 μM). This result suggested that EAK binds first to ODN molecules, followed by aggregate formation. The hydrodynamic diameter increased to 1000 and 2000 nm when the EAK concentration was increased to 60 and 90 μM , respectively. This might be due to the excess EAK binding to preformed EAK-ODN complexes, resulting in a further increase in diameter. Under the condition used in Fig. 9,

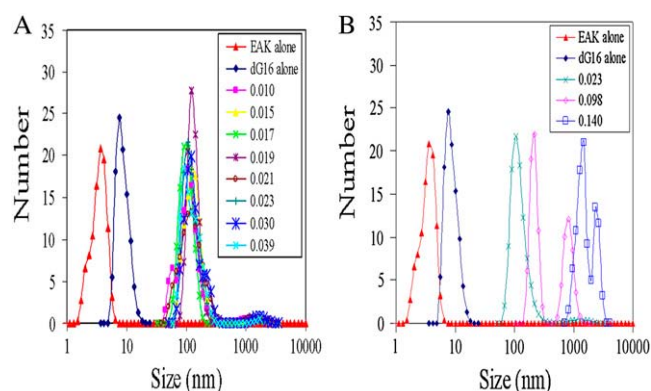


FIGURE 9 Population histogram of the EAK-ODN complexes as a function of particle diameter determined by dynamic light scattering. The EAK-ODN solutions contained $7.2 \mu\text{M}$ of dG_{16} with increasing EAK concentration at pH 4. The sample of EAK alone was measured 40 min after preparation, whose concentration was 0.1 mg/mL ($60 \mu\text{M}$). The concentration of dG_{16} alone was $7.2 \mu\text{M}$.

dG_{16} is fully incorporated in the EAK-ODN aggregates for an EAK concentration of $60 \mu\text{M}$, as shown in Fig. 1 (*open square*, Fig. 1). Since 0.1 mg/mL ($60 \mu\text{M}$) of EAK exhibited a size of $\sim 4 \text{ nm}$ 40 min after preparation (Fig. 9), it indicates that EAK does not self-assemble during that time and is present as single molecules. The observed large diameters in the EAK-ODN mixture solution are due to the aggregates of ODN and EAK in solution.

The results obtained by fluorescence anisotropy, SLS, and DLS all demonstrate that neither EAKs nor the ODNs self-assemble on their own within the first hour or so after sample preparation. Consequently the formation of EAK-ODN aggregates at pH 4 and pH 7 must result from the association of ODN and EAK unimers into complexes, which then self-assemble into aggregates (see Scheme I).

Binding parameters

The curves shown in Fig. 1 were used to generate plots of ν/P_f as a function of ν (Fig. 2). Equation 5 was used to obtain the binding constant, K , and the binding site size, n . The K - and n -values obtained for the binding of EAK to the ODNs at various pH values are listed in Table 3. As discussed in Theoretical Background, the association of the EAK-ODN complexes into aggregates is not accounted for by the MvH model. However the fits of ν/P_f versus ν with the MvH model shown in Fig. 2 are rather good.

It is observed in Fig. 1 that more EAK is required to form the same quantity of EAK-ODN aggregates when the pH is increased from 4 to 7, as a result of weaker electrostatic forces at pH 7. This observation is reflected quantitatively in Table 3, where the binding constant at pH 4 is 2.2-, 2.3-, and 6.0-folds larger than that at pH 7 for dG_{16} , dC_{16} , and dGC_{16} , respectively. The equilibrium constants obtained for the binding of EAK onto the ODNs range from 7.0×10^3 to

$7.6 \times 10^4 \text{ M}^{-1}$. In comparison, oligolysine and lysine-rich peptides such as KWK₆, K₄N₄, K₄N₆, and K_n ($n = 3-8$) have been reported to bind to oligo- and polynucleotides with binding constants in the range of $1 \times 10^3 \sim 1 \times 10^5 \text{ M}^{-1}$ (18,41,48,49). These values are comparable to those listed in Table 3.

The base composition of the ODN sequences, guanine in dG_{16} and cytosine in dC_{16} , appears to affect the binding of EAK to the ODNs since EAK binds more strongly to dG_{16} than to dC_{16} at both pH 4 and 7 (Table 3). Statistical analysis of protein-DNA complexes has established that Lys binds more readily to guanine (G) than to cytosine (C) (50). Binding of Lys to G occurs more effectively via hydrogen bonds to the two acceptors of the G base, whereas Lys binds preferentially to the phosphate oxygens of the C nucleotide. Furthermore, the study found that Lys has the highest propensity to interact with nucleotides, whereas Glu and Ala have the lowest (50). Since the interactions between nucleotides and glutamic acid are poor and since the favorable electrostatic forces between the negatively charged backbone of the ODNs and EAK are expected to be similar for dG_{16} and dC_{16} , the observation that dG_{16} binds more strongly to EAK than dC_{16} is rationalized by the enhanced formation of hydrogen bonds between the lysines of EAK and the guanines of dG_{16} .

The data listed in Table 3 indicate that EAK binds preferentially to ssODNs rather than to their duplex. This phenomenon has been observed for other peptides (12). This might be caused by the formation of hydrogen bonds between the amino acids of EAK and the nucleotide bases of ssODNs. This favorable interaction disappears in the case of dsODNs, since each nucleotide base hydrogen-bonds with the opposite base in the complementary strand of the duplex.

Solvent accessibility of ODNs in the EAK-ODN aggregates

One important aspect of the structure of the EAK-ODN aggregates is whether the ODNs are located inside or outside the aggregates. ODNs located inside the aggregates will be less accessible to the solvent than those located on the surface, and hence be protected from the outside environment. The accessibility of the ODN to the solvent was measured by performing fluorescence dynamic quenching experiments. dC_{16} was labeled either at the 5'-end with fluorescein (FAM- dC_{16} , $\lambda_{\text{ex}} = 452 \text{ nm}$, $\lambda_{\text{em}} = 514 \text{ nm}$) or at the 3'-end with rhodamine (dC_{16} -Rh, $\lambda_{\text{ex}} = 560 \text{ nm}$, $\lambda_{\text{em}} = 580 \text{ nm}$) to investigate whether both ends of dC_{16} are protected from the solvent. The fluorescence emission of a solution containing $3.6 \mu\text{M}$ of the labeled dC_{16} was monitored as the quencher KI was added to the solution in the presence or absence of 0.2 mg/mL EAK. Throughout these experiments, the potassium ion concentration was maintained constant and equal to 0.3 M by addition of K_2SO_4 to the KI solution, ensuring constant ionic strength.

As the KI concentration increased, the fluorescence intensity of fluorescein or rhodamine decreased. The I_0/I ratio was plotted as a function of iodide concentration in Fig. 10, *A* and *B*, for fluorescein and rhodamine, respectively. The quantities I_0 and I represent the fluorescence intensity of the chromophore without and with quencher, respectively. The I_0/I ratio was found to increase linearly with iodide concentration for both chromophores in the absence or presence of EAK. However, the increase was stronger in the absence of EAK.

The fluorescence decays of FAM-dC₁₆ and dC₁₆-Rh were acquired in the presence and absence of EAK. They were fitted with two exponentials according to Eq. 2. The preexponential factors and decay times obtained from the fits are listed in Table 4. Although fluorescein itself displays a single lifetime of 4.1 ns (51), the decay becomes more complex when fluorescein is covalently attached to an ODN where it shows two decay times. This phenomenon has been reported (52) to be due to a change in the conformation of fluorescein when it is covalently linked to an ODN. The binding of EAK onto the labeled ODN does not change the lifetime of the chromophore significantly as shown in Table 4.

To ensure that the quenching is dynamic, the fluorescence decays of the FAM-dC₁₆-EAK mixture were acquired in the absence and presence of 0.2 M KI. The average lifetime of the decays was determined and the ratio of the average lifetime of the solution without KI (τ_0) over that of the solution with 0.2 M KI (τ) was found to be 1.8, i.e., $\tau_0/\tau = 1.8$. The I_0/I ratio obtained from the steady-state fluorescence measurements equaled 1.9 for a concentration of 0.2 M KI, a value comparable to the τ_0/τ ratio. The agreement obtained between the I_0/I and τ_0/τ ratios strongly suggests that the quenching is dynamic (37). Fitting the I_0/I versus $[I^-]$ trends shown in Fig. 10 with the Stern-Volmer equation given in Eq. 6 yields the bimolecular quenching rate constant, k_q , which reflects the accessibility of the chromophore to the solvent (37),

$$I_0/I = 1 + K_{SV}[Q] = 1 + k_q\tau_0[Q]. \quad (6)$$

The slopes of the straight lines referred to as the Stern-Volmer constants, K_{SV} , are listed in Table 5. As indicated in Eq. 6, k_q is determined from the ratio K_{SV}/τ_0 where τ_0 is the lifetime of the chromophore in the absence of quencher (37).

Since the fluorescence decay of the chromophores without quencher is biexponential, the average lifetime $\bar{\tau}_0$ was used

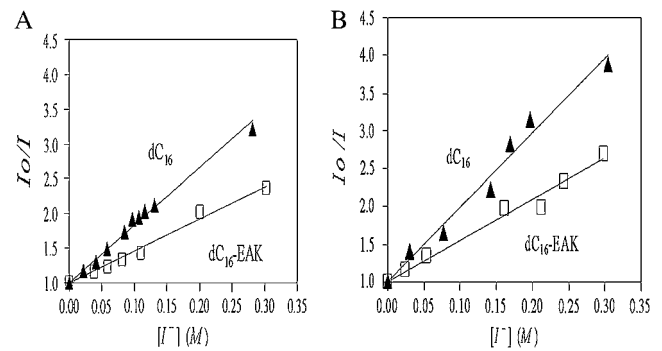


FIGURE 10 Stern-Volmer plots for a solution of 3.6 μ M of fluorescently-labeled dC₁₆ free and bound to 0.2 mg/mL of EAK at pH 4 quenched by KI. Solid lines represent the fits to the Stern-Volmer equation with parameters listed in Table 5. (A) FAM-dC₁₆ (\blacktriangle), FAM-dC₁₆-EAK (\square); and (B) dC₁₆-Rh (\blacktriangle), and dC₁₆-Rh-EAK (\square).

to calculate the bimolecular quenching rate constant k_q from the slope K_{SV} of the plots in Fig. 10. The values of K_{SV} , $\bar{\tau}_0$, and k_q are listed in Table 5. In the absence of EAK, k_q for FAM-dC₁₆ and dC₁₆-Rh equals $2.5 \times 10^9 \text{ M}^{-1} \text{ s}^{-1}$ and $3.5 \times 10^9 \text{ M}^{-1} \text{ s}^{-1}$, respectively. The bimolecular quenching rate constant is related to the quenching efficiency, size, and diffusion coefficient of the chromophore and quencher. Since the iodide ions have quenching efficiencies near unity (37) and the overall sizes of the two labeled ODNs are comparable, the differences in k_q found for FAM-dC₁₆ and dC₁₆-Rh (Table 5) must reflect differences in the efficiency of iodide at quenching the excited chromophores. Indeed, FAM and Rh are neutral and positively charged at pH 4, respectively. Considering electrostatic forces alone, the negatively charged iodide ions are expected to quench more efficiently to Rh than FAM. In addition, FAM is expected to be less mobile than Rh as an 8- and 12-atom linker connects the 5'-end and the 3'-end phosphate groups of dC₁₆ to FAM and Rh, respectively. In the presence of EAK, k_q decreases for both FAM-dC₁₆ and dC₁₆-Rh. For FAM-dC₁₆, k_q decreases from $2.5 \times 10^9 \text{ M}^{-1} \text{ s}^{-1}$ to $1.5 \times 10^9 \text{ M}^{-1} \text{ s}^{-1}$. Similarly, for dC₁₆-Rh, k_q decreases from $3.5 \times 10^9 \text{ M}^{-1} \text{ s}^{-1}$ to $2.0 \times 10^9 \text{ M}^{-1} \text{ s}^{-1}$. Considering the diffusion coefficient of the fluorophore-labeled ODN of 16 bases would be $\sim 1.3 \times 10^{-6} \text{ cm}^2/\text{s}$ (53), which is 10-fold lower than that of iodide ion with $1.9 \times 10^{-5} \text{ cm}^2/\text{s}$ (54), k_q will be affected at most 10% by the diminution of the diffusion coefficient of the ODNs after incorporation in the EAK-ODN aggregates.

TABLE 4 Preexponential factors and decay times obtained from the analysis of the fluorescence decays of the fluorescent ODNs in the absence and presence of EAK in pH 4 buffer, respectively

	τ_1 (ns)	α_1	τ_2 (ns)	α_2	$\bar{\tau}$ (ns)*	χ^2
FAM-dC ₁₆ (without KI)	3.9	0.67	2.0	0.33	3.3	1.12
EAK-FAM-dC ₁₆ (without KI)	3.7	0.63	1.7	0.37	3.0	1.00
EAK-FAM-dC ₁₆ (with KI)	2.8	0.43	1.0	0.57	1.7	1.15
dC ₁₆ -Rh (without KI)	3.9	0.60	1.5	0.40	2.9	1.13
EAK-dC ₁₆ -Rh (without KI)	3.8	0.58	1.3	0.42	2.8	1.37

* $\bar{\tau}$ is the number average lifetime, given by $\bar{\tau} = \sum \tau_i \alpha_i / \sum \alpha_i$.

TABLE 5 Stern-Volmer quenching constants K_{SV} , bimolecular quenching rate constant k_q , fluorescence lifetime τ_o , and relative accessibility change γ when dC₁₆ is in the absence or presence of 0.2 mg/mL of EAK in pH 4 buffer

ODNs	5'-End fluorescein labeling				3'-End rhodamine labeling			
	K_{SV} (M ⁻¹)	τ_o (ns)	k_q (10 ⁹ M ⁻¹ s ⁻¹)	γ	K_{SV} (M ⁻¹)	τ_o (ns)	k_q (10 ⁹ M ⁻¹ s ⁻¹)	γ
Fluorescently-labeled dC ₁₆ (free)	8.3 ± 0.2	3.3	2.5 ± 0.1		9.9 ± 0.4	2.8	3.5 ± 0.1	
Fluorescently-labeled EAK-dC ₁₆ (bound)	4.6 ± 0.1	3.0	1.5 ± 0.1	0.60	5.5 ± 0.2	2.7	2.0 ± 0.1	0.57

Thus, the decrease in k_q observed in Table 5 (~40%) suggests that the accessibility of ODNs must be reduced after binding to EAK.

The change in accessibility of the ODNs upon EAK binding was quantified with the relative accessibility change, γ , defined by (34)

$$\gamma = k_q^b/k_q^f, \quad (7)$$

where k_q^b and k_q^f are the bimolecular quenching constants for the chromophore-labeled ODNs in the presence and absence of EAK, respectively. The values of γ for the two different labels are listed in Table 5. The relative accessibility changes of dC₁₆ for both types of labels are similar and smaller than unity, being 0.60 and 0.57 for the 5'-labeled FAM-dC₁₆ and the 3'-labeled dC₁₆-Rh, respectively. Since γ is smaller than 1.0, the accessibility of the 5'- and 3'-ends of dC₁₆ to the solvent is reduced after the binding of EAK to dC₁₆. Since the γ -values corresponding to the two labels are similar, the accessibility of both ends of dC₁₆ to the solvent is reduced by the same extent, ~40%. The fact that different sections of the ODN exhibit a similar reduction in accessibility suggests that the entire ODN molecule is protected by the EAK molecules inside the EAK-ODN aggregates.

It is worth noting that while the negatively charged ODNs should repel the quencher (I⁻), the negative charges on the ODNs are, at least partially, neutralized by the positively charged EAK in the EAK-ODN aggregates. Consequently the iodide ions would be expected to be more efficient at colliding with the ODNs in the presence of EAK. Interestingly the opposite is observed, which strengthens the claim that EAK protects the ODN from its environment.

Unprotected ODNs are rapidly degraded in vitro and in vivo due to the presence of nucleases. The reduction of accessibility to the solvent experienced by the ODNs upon assembly with EAK suggests that the degradation of the complexed ODN will be reduced when used in biological systems. Further investigations are underway to verify the stability of the EAK-ODN aggregates and the potential of ODN encapsulation by EAK for oligonucleotide delivery.

CONCLUSIONS

In this work the molecular interaction of EAK with ODNs in solution was studied by a number of physicochemical methods. UV-Vis absorption experiments showed that the binding between EAK and ODNs resulted in the formation of

EAK-ODN aggregates that could be centrifuged out. Fluorescence anisotropy, PAGE, and UV-Vis experiments demonstrated that EAK-ODN complexes, as well as EAK and ODN unimers, existed in the supernatant of the centrifuged EAK-ODN mixtures. The binding isotherms between EAK and ODNs were established from the UV-Vis absorption results through a binding density function analysis. Fluorescence anisotropy and static light scattering experiments showed that the process of EAK binding to ODNs started with EAK-ODN molecular complexation, followed by association of the complexes into aggregates. For comparison purposes, the binding isotherm was fitted with the modified noncooperative MvH model to extract the equilibrium binding constants. The binding was found to be strongest at pH 4. No binding was observed at pH 11. The equilibrium binding constant decreases two-to-sixfold when the pH changes from 4 to 7. Since the equilibrium binding constant decreases as EAK becomes less positively charged, the interaction between EAK and ODNs must occur mainly via electrostatic interactions, but hydrogen bonding between EAK and the nucleotides of the ODNs may also be involved. Hydrogen bonds are believed to promote the binding of EAK to dG₁₆ to a greater extent than to dC₁₆. Furthermore, EAK has a slight preference to bind with the ssODNs than to the dsODN.

The size of EAK-ODN aggregates was determined by AFM and DLS, and found to equal ~150 nm at low EAK concentrations. Fluorescence quenching experiments showed that the accessibility of ODNs to the solvent was reduced upon EAK binding. EAK-ODN aggregates can protect the ODNs from encountering the quencher in the surrounding solvent.

SUPPLEMENTARY MATERIAL

To view all of the supplemental files associated with this article, visit www.biophysj.org.

We thank Hye-Young Suk for her assistance with data collection and Dan Anderson for stimulating discussions.

This research was financially supported by the Natural Sciences and Engineering Research Council of Canada, the Canadian Foundation for Innovation, and the Canadian Research Chairs program. J.D. is particularly thankful to the funding of an Ontario's Premier Research Excellence Award.

REFERENCES

- Zhang, S., T. C. Holmes, C. Lockshin, and A. Rich. 1993. Spontaneous assembly of a self-complementary oligopeptide to form a stable macroscopic membrane. *Proc. Natl. Acad. Sci. USA.* 90:3334-3338.

2. Chen, P. 2005. Self-assembly of ionic-complementary peptides: a physicochemical viewpoint. *Colloids Surf. A*. 261:3–24.
3. Zhang, S. 2002. Emerging biological materials through molecular self-assembly. *Biotechnol. Adv.* 20:321–339.
4. Aggeli, A., N. Boden, and S. Zhang. 1999. Self-assembly of peptides in medicine: two sides of the coin. *Mol. Med. Today*. 5:512–513.
5. Zhang, S., C. Lockshin, R. Cook, and A. Rich. 1994. Unusually stable beta-sheet formation in an ionic self-complementary oligopeptide. *Biopolymers*. 34:663–672.
6. Hong, Y., R. L. Legge, S. Zhang, and P. Chen. 2003. Effect of amino acid sequence and pH on nanofiber formation of self-assembling peptides EAK16-II and EAK16-IV. *Biomacromolecules*. 4:1433–1442.
7. Fung, S. Y., C. Keyes, J. Duhamel, and P. Chen. 2003. Concentration effect on the aggregation of a self-assembling oligopeptide. *Biophys. J.* 85:537–548.
8. Zhang, S., T. C. Holmes, M. Dipersio, R. O. Hynes, X. Su, and A. Rich. 1995. Self-complementary oligopeptide matrices support mammalian cell attachment. *Biomaterials*. 16:1385–1393.
9. Holmes, T. C., S. D. Lacelle, X. Su, G. Liu, A. Rich, and S. Zhang. 2000. Extensive neurite outgrowth and active synapse formation on self-assembling peptide scaffolds. *Proc. Natl. Acad. Sci. USA*. 97:6728–6733.
10. Keyes-Bag, C., S. Y. Fung, J. Bezaire, and P. Chen. 2004. Self-assembling peptide as a potential carrier of hydrophobic compounds. *J. Am. Chem. Soc.* 126:7522–7532.
11. Plank, C., M. X. Tang, A. R. Wolfe, and F. C. Szoka. 1999. Branched cationic peptides for gene delivery: role of type and number of cationic residues in formation and *in vitro* activity of DNA polyplexes. *Hum. Gene Ther.* 10:319–332.
12. Simeoni, F., M. C. Morris, F. Heitz, and G. Divita. 2003. Insight into the mechanism of the peptide-based gene delivery system MPG: implications for delivery of siRNA into mammalian cells. *Nucleic Acids Res.* 31:2717–2724.
13. Bergen, J. M., and S. H. Pun. 2005. Peptide-enhanced gene delivery. *MRS Bull.* 30:663–667.
14. Schwarz, G., and F. Watanabe. 1983. Thermodynamics and kinetics of cooperative protein-nucleic acid binding. I. General aspects of analysis of data. *J. Mol. Biol.* 163:467–484.
15. McGhee, J. D., and P. H. von Hippel. 1974. Theoretical aspects of DNA-protein interactions: cooperative and noncooperative binding of large ligands to a one-dimensional homogeneous lattice. *J. Mol. Biol.* 86:469–489.
16. Muller, R., T. Restle, J. Reinstein, and R. S. Goody. 1991. Interaction of fluorescently labeled dideoxynucleotides with HIV-1 reverse transcriptase. *Biochemistry*. 30:3709–3715.
17. Scatchard, G. 1949. The attractions of proteins for small molecules and ions. *Ann. N. Y. Acad. Sci.* 51:660–672.
18. Latt, S. A., and H. A. Sober. 1967. Protein-nucleic acid interactions. II. Oligopeptide-polyribonucleotide binding studies. *Biochemistry*. 6:3293–3306.
19. Crothers, D. M. 1968. Chain transfer for vinyl monomers polymerized in N-allylstearamide. *Biopolymers*. 6:575–584.
20. Schwarz, G. 1970. Cooperative binding to linear biopolymers. 1. Fundamental static and dynamic properties. *Eur. J. Biochem.* 12:442–453.
21. Epstein, I. R. 1978. Cooperative and non-cooperative binding of large ligands to a finite one-dimensional lattice. A model for ligand-oligonucleotide interactions. *Biophys. J.* 8:327–339.
22. Tsodikov, O. V., J. A. Holbrook, I. A. Shkel, and M. T. Record. 2001. Analytic binding isotherms describing competitive interactions of a protein ligand with specific and nonspecific sites on the same DNA oligomer. *Biophys. J.* 81:1960–1969.
23. Bujalowski, W., and T. M. Lohman. 1987. A general method of analysis of ligand-macromolecule equilibria using a spectroscopic signal from the ligand to monitor binding. Application to *E. coli* SSB protein-nucleic acid interactions. *Biochemistry*. 26:3099–3106.
24. Morii, T., J. Yamane, Y. Aizawa, K. Makino, and Y. Sugiura. 1996. Cooperative oligomerization enhances sequence-selective DNA binding by a short peptide. *J. Am. Chem. Soc.* 116:10011–10017.
25. Stierle, V., J. Couprie, C. Ostlund, I. Krimm, S. Zinn-Justin, P. Hossenlopp, H. J. Worman, J. C. Courvalin, and I. Duband-Goulet. 2003. The carboxyl-terminal region common to lamins A and C contains a DNA binding domain. *Biochemistry*. 42:4819–4828.
26. Agou, F., S. Raveh, S. Mesnildrey, and M. Veron. 1999. Single strand DNA specificity analysis of human nucleoside diphosphate kinase B. *J. Biol. Chem.* 274:19630–19638.
27. Seimiya, M., and Y. Kurosawa. 1996. Kinetics of binding of Antp homeodomain to DNA analyzed by measurements of surface plasmon resonance. *FEBS Lett.* 398:279–284.
28. Endoh, T., H. Funabashi, M. Mie, and E. Kobatake. 2005. Method for detection of specific nucleic acids by recombinant protein with fluorescent resonance energy transfer. *Anal. Chem.* 77:4308–4314.
29. Michel, S. L., A. L. Guerrero, and J. M. Berg. 2003. Selective RNA binding by a single CCCH zinc-binding domain from Nup475 (Tristetraprolin). *Biochemistry*. 42:4626–4630.
30. Galletto, R., M. J. Jezewska, and W. Bujalowski. 2003. Interactions of the *Escherichia coli* DnaB helicase hexamer with the replication factor the DnaC protein. Effect of nucleotide cofactors and the ssDNA on protein-protein interactions and the topology of the complex. *J. Mol. Biol.* 329:441–465.
31. Boraston, A. B., P. Chiu, R. A. J. Warren, and D. G. Kilburn. 2000. Specificity and affinity of substrate binding by a family 17 carbohydrate-binding module from *Clostridium cellulovorans* cellulase 5A. *Biochemistry*. 39:11129–11136.
32. Jensen, D. E., and P. H. von Hippel. 1977. A boundary sedimentation velocity method for determining nonspecific nucleic acid-protein interaction binding parameters. *Anal. Biochem.* 80:267–281.
33. Creagh, A. L., E. Ong, E. Jervis, D. G. Kilburn, and C. A. Haynes. 1996. Binding of the cellulose-binding domain of exoglucanase Cex from *Cellulomonas fimi* to insoluble microcrystalline cellulose is entropically driven. *Proc. Natl. Acad. Sci. USA*. 93:12229–12234.
34. Bujalowski, W., and M. M. Klonowaka. 1994. Structural characteristics of the nucleotide-binding site of *Escherichia coli* primary replicative helicase DnaB protein. Studies with ribose and base-modified fluorescent nucleotide analogs. *Biochemistry*. 33:4682–4694.
35. Akinrimisi, E. O., C. Sander, and P. O. P. Ts'o. 1963. Properties of helical polycytidylic acid. *Biochemistry*. 2:340–344.
36. Bolumar, T., T. Y. Sanz, M. C. Aristoy, and F. Toldra. 2003. Purification and characterization of a prolyl aminopeptidase from *Debaryomyces hansenii*. *Appl. Environ. Microbiol.* 69:227–232.
37. Lakowicz, J. R. 1999. Principles of Fluorescence Spectroscopy. Plenum Press, New York.
38. Press, W. H., B. P. Flannery, S. A. Teukolsky, and W. T. Vetterling. 1992. Numerical Recipes. The Art of Scientific Computing. Cambridge University Press, Cambridge, UK.
39. Teif, V. B., and D. Y. Lando. 2001. Calculations of DNA condensation caused by ligand adsorption. *Mol. Biol.* 35:106–107.
40. Teif, V. B. 2005. Ligand-induced DNA condensation: choosing the model. *Biophys. J.* 89:2574–2587.
41. Ballin, J. D., I. A. Shkel, and M. T. Record. 2004. Interactions of the KWK6 cationic peptide with short nucleic acid oligomers: demonstration of large Coulombic end effects on binding at 0.1–0.2 M salt. *Nucleic Acids Res.* 32:3271–3281.
42. Casas-Finet, J. R., J. D. Smith, A. Kumar, J. G. Kim, S. H. Wilson, and R. L. Karpel. 1993. Mammalian heterogeneous ribonucleoprotein A1 and its constituent domains: nucleic acid interaction, structural stability and self-association. *J. Mol. Biol.* 229:873–889.
43. Lehninger, A. L. 1993. Principles of Biochemistry. Worth Publishers, New York.
44. Gottschalk, S., J. T. Sparrow, J. Hauer, M. P. Mims, F. E. Leland, and S. Woo. 1996. A novel DNA-peptide complex for efficient gene transfer and expression in mammalian cells. *Gene Ther.* 3:448–457.

45. Hamman, B. D., A. V. Oleinikov, G. G. Jokhadze, D. E. Bochkariov, R. R. Traut, and D. M. Jameson. 1996. Tetramethylrhodamine dimer formation as a spectroscopic probe of the conformation of *Escherichia coli* ribosomal protein L7/L12 dimers. *J. Biol. Chem.* 271:7568–7573.
46. Förster, T., and E. König. 1957. Absorption spectra and fluorescence characteristics of concentrated solutions of organic coloring materials. *Z. Elektrochem.* 61:344–348.
47. Sambrook, J., E. F. Fritsch, and T. Maniatis. 1989. *Molecular Cloning: A Laboratory Manual*, 2nd Ed. Cold Spring Harbor Laboratory Press, Cold Spring Harbor, NY.
48. Matsuno, H., K. Niikura, and Y. Okahata. 2001. Design and characterization of asparagine- and lysine-containing alanine-based helical peptides that bind selectively to A·T base pairs of oligonucleotides immobilized on a 27 MHz quartz crystal microbalance. *Biochemistry.* 40:3615–3622.
49. Roy, K. B., S. Kukreti, H. S. Bose, V. S. Chauhan, and M. R. Rajeswari. 1992. Hairpin and duplex forms of a self-complementary dodecamer, d-AGATCTAGATCT, and interaction of the duplex form with the peptide KGWGK: can a pentapeptide destabilize DNA? *Biochemistry.* 31:6241–6245.
50. Lejeune, D., N. Delsaux, B. Charlotiaux, A. Thomas, and R. Brasseur. 2005. Protein-nucleic acid recognition: statistical analysis of atomic interactions and influence of DNA structure. *Proteins.* 61:258–271.
51. Sjoback, R., J. Nygren, and M. Kubista. 1995. Absorption and fluorescence properties of fluorescein. *Spectrochim. Acta [A]*. 51:L7–L21.
52. Sjoback, R., J. Nygren, and M. Kubista. 1998. Characterization of fluorescein-oligonucleotide conjugates and measurement of local electrostatic potential. *Biopolymers.* 46:445–453.
53. Gordan, S. P., S. Berezina, D. Scherfeld, N. Kahya, and P. Schwill. 2005. Characterization of interaction between cationic lipid-oligonucleotide complexes and cellular membrane lipids using confocal imaging and fluorescence correlation spectroscopy. *Biophys. J.* 88: 305–316.
54. Weast, R. C. 1971. *Handbook of Chemistry and Physics*. P. F47. The Chemical Rubber Co., Cleveland, OH.